C. R. Physique 15 (2014) 630–639

Contents lists available at ScienceDirect

Comptes Rendus Physique

www.sciencedirect.com

Emergent phenomena in actinides / Phénomènes émergents dans les actinides

Spin fluctuation and Fermi surface instability in ferromagnetic superconductors

Fluctuation de spins et instabilité de la surface de Fermi dans les supraconducteurs ferromagnétiques

Dai Aoki [a,b,*], Adrien Gourgout [b], Alexandre Pourret [b], Gaël Bastien [b], Georg Knebel [b], Jacques Flouquet [b]

[a] *IMR, Tohoku University, Oarai, Ibaraki, 311-1313, Japan*
[b] *SPSMS, UMR-E CEA/UJF-Grenoble 1, INAC, 38054 Grenoble, France*

ARTICLE INFO

Article history:
Available online 8 August 2014

Keywords:
Heavy fermion
Unconventional superconductivity
Ferromagnetism
UGe_2
UCoGe
URhGe

Mots-clés :
Fermions lourds
Supraconductivité non conventionnelle
Ferromagnetism
UGe_2
UCoGe
URhGe

ABSTRACT

We review the ferromagnetic superconductivity observed in the uranium based compounds, namely UGe_2, URhGe and UCoGe, where the spin-triplet state is most likely realized. An unusual upper critical field H_{c2}, which is enhanced under a magnetic field in a certain field direction, is discussed in terms of spin fluctuations and of Fermi surface instabilities.

RÉSUMÉ

Dans cet article, on présente une revue des supraconducteurs ferromagnétiques à base d'uranium, tels UGe_2, URhGe et UCoGe, dans lesquels l'état fondamental est un triplet de spin. Le champ critique supérieur H_{c2} a un comportement non usuel dans ces composés et croît en présence d'un champ magnétique appliqué le long de certaines directions. Ce phénomène est discuté en termes de fluctuations de spin et d'instabilités de la surface de Fermi.

1. Introduction

The coexistence of ferromagnetism (FM) and superconductivity (SC) attracts much interest, because unconventional SC is expected [1]. In the conventional *s*-wave SC, FM impedes the formation of Cooper pairs, because the large internal field is not compatible with the spin-singlet state. In several rare-earth compounds, such as Chevrel phase compound $ErRh_4B_4$ [2], the Curie temperature T_{Curie} is observed below the superconducting transition temperature T_{sc}, but SC basically conflicts with FM. Once FM state is established, SC is destroyed. The ordered moment of the rare-earth atom is also large, indicating localized 4f-electrons, which does not allow carrying conduction electrons.

* Corresponding author.

http://dx.doi.org/10.1016/j.crhy.2014.07.004
1631-0705/

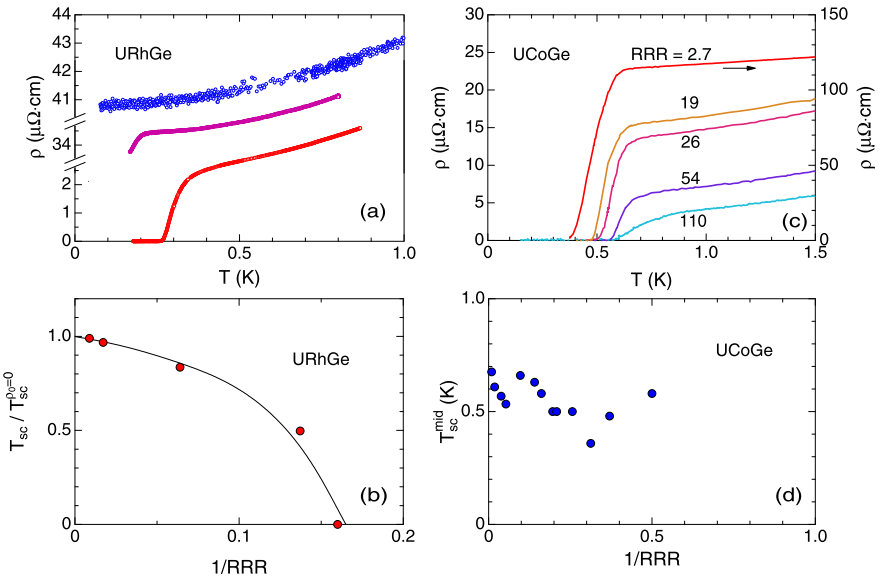

Fig. 1. (Color online.) Temperature dependence of resistivity with different RRR in (a) URhGe [12] and (c) UCoGe. T_{sc} vs 1/RRR in (b) URhGe and (d) UCoGe. T_{sc} in URhGe is normalized with T_{sc} for $\rho_0 \to 0$. T_{sc} in URhGe was defined by the onset of SC in resistivity. T_{sc} in UCoGe is defined as a mid-point of the resistivity drop.

On the other hand, the microscopic coexistence of FM and SC is known in uranium compounds, namely UGe_2 [3], URhGe [4] and UCoGe [5]. Although the FM ordered moments in the SC state vary from 1 to $0.05\,\mu_B$/U, the 5f electrons are considered to be itinerant at first approximation, because the moment is much smaller than the free ion value.

UGe_2 orders ferromagnetically below $T_{Curie} = 52$ K. Applying the pressure, T_{Curie} is suppressed at $P_c = 1.5$ GPa. The SC phase appears just below P_c with the maximum $T_{sc} = 0.8$ K at another critical pressure $P_x \sim 1.2$ GPa, where T_x is suppressed. T_x is the boundary between the weakly polarized FM phase (FM1) and the strongly polarized FM phase (FM2). At ambient pressure, T_x is a crossover between FM1 and FM2; it changes into the first-order transition through the critical end point (CEP). T_{Curie} also changes from the second-order transition to the first-order transition at the tricritical point (TCP) at $P_{TCP} \sim 1.42$ GPa and at $T_{TCP} \sim 24$ K. Applying a field, the critical temperature can be tuned to 0 K, showing the so-called wing structure in the temperature–pressure–field phase diagram [6,7].

URhGe is a ferromagnet with $T_{Curie} = 9.5$ K. The ordered moment ($0.4\,\mu_B$) is smaller than that of UGe_2 ($1.5\,\mu_B$). SC is observed at ambient pressure at $T_{sc} = 0.25$ K. With increasing pressure, T_{Curie} increases, while T_{sc} decreases [8], indicating that the system goes far from the critical region by pressure. The Sommerfeld specific heat coefficient is $\gamma = 160$ mJ K^{-2} mol^{-1}, which indicates a moderately enhanced heavy electronic state.

UCoGe also shows a ferromagnetic transition at $T_{Curie} \sim 3$ K, with the ordered moment $0.05\,\mu_B$. SC is found at $T_{sc} \sim 0.7$ K. T_{Curie} decreases with pressure and becomes 0 K at the critical pressure $P_c \sim 1.2$ GPa [9,10]. On the other hand, T_{sc} increases with a broad maximum around P_c, and then decreases. The SC state appears in both the FM and PM states. The initial γ-value (55 mJ K^{-2} mol^{-1}) also shows a maximum at P_c, according to the analysis of the resistivity coefficient A.

An interesting point is that the crystal structure of the three ferromagnetic superconductors forms a zigzag chain of U atoms. UGe_2 has an orthorhombic structure with the space group *Cmmm*. The distance of the first nearest neighbor of U is $d_{U\text{-}U} = 3.85$ Å. The zigzag chain is elongated along the *a*-axis and the moment is also directed along the *a*-axis. URhGe and UCoGe have the same orthorhombic crystal structure, with the space group *Pnma*. The zigzag chain is elongated along *a* and the moment is directed along the *c*-axis. The value of $d_{U\text{-}U}$ is 3.50 Å in URhGe and 3.48 Å in UCoGe, which is close to the so-called Hill limit. It should be noted that these structures of UGe_2, URhGe and UCoGe have the inversion symmetry in global, but no inversion symmetry in local due to the zigzag chain. It is pointed out that interesting phenomena are expected owing to the parity mixing and the strong spin–orbit interactions. In URhGe, weak antiferromagnetism, which can be induced by the Dzyaloshinskii–Moriya interaction, is theoretically predicted [11].

2. Sample quality and T_{sc}

URhGe and UCoGe are materials with which it is very difficult to grow high-quality single crystals using the Czochralski method, because they have an incongruent melting. Other attempts at crystal growth, such as the flux method and the Bridgeman method, have so far been unsuccessful. Fig. 1b shows the variation of T_{sc} as a function of the inverse residual resistivity ratio (RRR) in URhGe polycrystalline samples, which are obtained from different annealing conditions [12]. T_{sc} is very sensitive to the sample quality, and decreases with increasing residual resistivity. T_{sc} should be basically described by

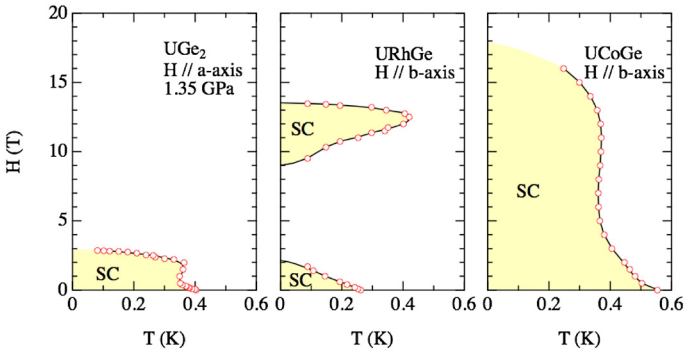

Fig. 2. (Color online.) Field–temperature phase diagram for SC in UGe_2, URhGe and UCoGe. The field is applied along the easy-magnetization axis (a-axis) in UGe_2 at pressures between P_x and P_c. In URhGe and UCoGe, the field is applied along the hard magnetization axis (b-axis) [19].

Abrikosov–Gorkov's pair-breaking theory, which is valid not only for magnetic impurities, but also for non-magnetic ones, as observed in Sr_2RuO_4 [13]. The strong dependence of T_{sc} on the sample quality indicates that SC is unconventional in URhGe.

In UCoGe, T_{sc} is not as sensitive to the sample quality as in URhGe, as shown in Fig. 1d, contrary to the FM, which is strongly affected by sample quality. UCoGe is close to an FM instability already at ambient pressure, the FM phase is easily suppressed at small pressure, $P_c \sim 1.2$ GPa. T_{sc} shows a broad maximum around P_c with increasing pressure, indicating SC in both the FM sate and the PM state as a function of pressure. NQR spectra measured on polycrystalline samples at ambient pressure show two different states, namely FM and PM, indicating phase separation [14]. As the FM transition displays a first-order-like behavior and UCoGe is close to the FM instability, the phase separation of FM and PM states is possible. An interesting point is that NQR spectra arising from both the FM and the PM states show SC to be temperature-dependent on T_1. The FM state dominates in the higher-quality samples, while the fraction of PM phase due to the phase separation increases in lower-quality samples. Since both phases become superconducting, the T_{sc} of UCoGe seems insensitive to sample quality, compared to that of URhGe. It is also noted that the SC of UCoGe is detected even in Si-substituted compounds up to 10% [15], indicating that the SC of UCoGe is insensitive to sample quality.

3. Field-reinforced superconductivity

One of the most spectacular behaviors in ferromagnetic superconductors is the unusual temperature dependence of H_{c2}. Fig. 2 shows the H_{c2} curves in UGe_2 [16], URhGe [17] and UCoGe [18]. In UGe_2, the pressure is varied between $P_c \sim 1.5$ GPa and $P_x \sim 1.2$ GPa. For UGe_2, the field is applied along the easy-magnetization axis ($H \parallel a$-axis), whereas the field is applied along the hard-magnetization axis ($H \parallel b$-axis) in URhGe and UCoGe. In these three materials, H_{c2} at 0 K is much higher than the value expected from the Pauli-paramagnetic limit based on the weak-coupling BCS model ($H_P \sim 1.86 T_{sc}$), which means that the spin-triplet state with equal-spin pairing is most likely realized, where H_{c2} is not governed by the Pauli-paramagnetic limit.

Furthermore, unusual "S"-shaped or field-reentrant H_{c2} curves are shown by the three materials. In UGe_2, it is known that the FM state changes from FM1 to FM2 at the metamagnetic field H_x where H_{c2} increases vertically. The dHvA experiments show a drastic change of the Fermi surface between the FM1, FM2, and PM states. The Sommerfeld coefficient also shows a large drop at H_x with increasing the field. The changes of Fermi surface and effective mass are key ingredients for the S-shaped H_{c2} in UGe_2.

In URhGe reentrant SC occurs between ∼9 and ∼13.5 T. Surprisingly, $T_{sc} = 0.4$ K at 12.5 T is higher than $T_{sc} = 0.25$ K at zero field, indicating that the SC is indeed reinforced by the magnetic field.

A similar behavior is also observed in UCoGe. The temperature dependence of H_{c2} shows the S-shaped curve instead of reentrant SC phase. T_{sc} at zero field in UCoGe is twice as large as in URhGe, thus the low-field SC phase is widened. One can consider that the low-field SC phase and the reentrant SC phase are merged in UCoGe. As a result, the S-shaped H_{c2} curve is observed.

The similarity of URhGe and UCoGe is also seen in the field–temperature phase diagram for the Curie temperature. As shown in Fig. 3, T_{Curie} is suppressed with the field in the transverse configuration, where the field is applied perpendicular to the initial easy-magnetization axis. According to the GL free energy consideration [20], it is known that T_{Curie} is suppressed with the field, following $\Delta T_{Curie} \propto -H^2$, when the field is applied along the hard-magnetization axis. Usually, it is difficult to observe experimentally the suppression of T_{Curie} with the field, because T_{Curie} under a field gets easily smeared due to the small mis-orientation of the easy-axis. Even if the single-crystal sample is perfectly aligned to the hard-axis, T_{Curie} is almost unchanged with the field up to the upper experimental limit because of the strong Ising anisotropy. URhGe is a special case, because the moment can be easily tilted from the c to the b-axis with increasing the field. The magnetization curve also shows this peculiar behavior, namely the initial slope of magnetization (dM/dH) for $H \parallel b$-axis is rather large, as shown in Fig. 4a. The value of dM/dH for the b-axis is larger than that for the $H \parallel c$-axis, thus the spin reorientation to the b-axis occurs at $H_R \sim 12$ T.

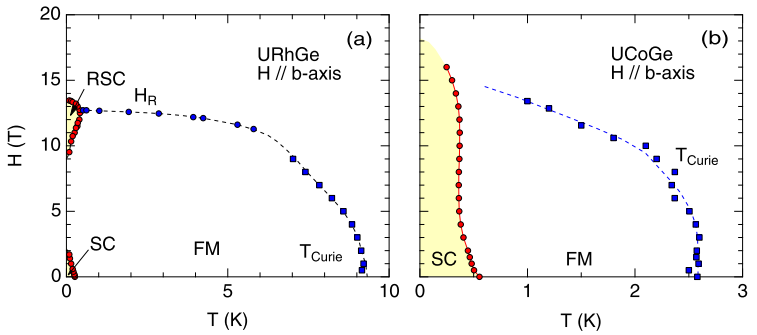

Fig. 3. (Color online.) Field–temperature phase diagram in URhGe and UCoGe for the $H \parallel b$-axis [19].

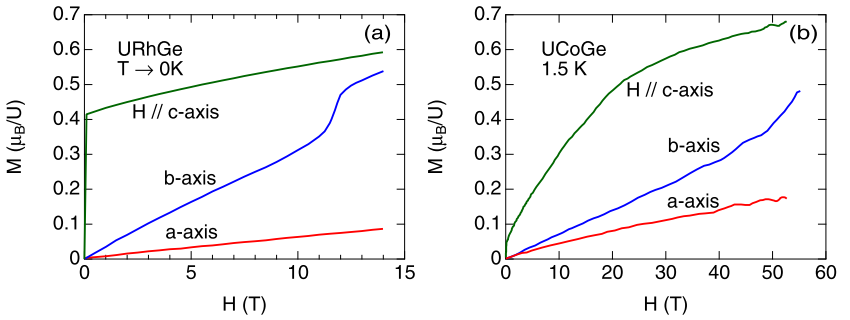

Fig. 4. (Color online.) Magnetization curves for a, b and c-axis in URhGe [21] and UCoGe [22].

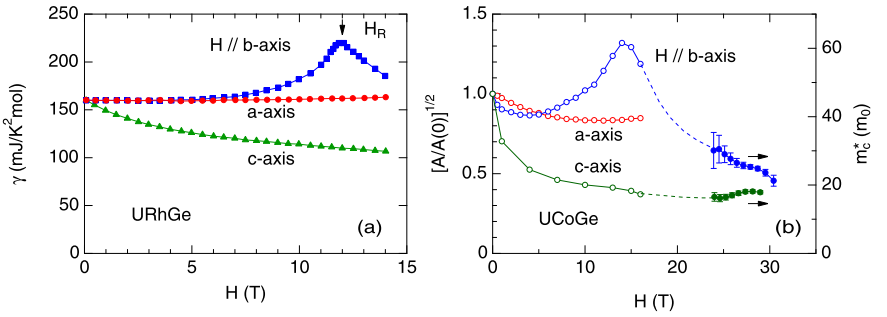

Fig. 5. (Color online.) Field dependence of effective mass detected by its Sommerfeld coefficient in URhGe [21] and the resistivity A coefficient in the form of $[A(H)/A(0)]^{1/2}$ vs. H in UCoGe. The field dependence of the cyclotron effective mass from SdH experiments is also plotted for UCoGe [19].

UCoGe also shows a similar field–temperature phase diagram. T_{Curie} is suppressed from 2.5 K to 0 K around 14 T. The significant difference is that no spin-reorientation is detected at high fields in UCoGe. The magnetization curve shows no step-like anomaly, but increases linearly, as shown in Fig. 4b. The ordered moment of UCoGe is very small ($\sim 0.05\,\mu_B$), indicating weak itinerant ferromagnetism. The increase of magnetization with increasing the field for the $H \parallel c$-axis is more significant than that for the $H \parallel b$-axis. This is why UCoGe does not show the spin reorientation for the $H \parallel b$-axis. The high-field magnetization up to 55 T for $H \parallel b$-axis shows the upward curvature around 50 T. This broad anomaly is not connected to T_{Curie} at zero field, but most likely vanishes at 30–40 K, where the susceptibility shows a broad maximum, indicating that the broad anomaly at 50 T is probably due to the spin polarization at high field rather than to a spin reorientation.

4. Mass enhancement and H_{c2}

The FM instabilities at high field induce the mass enhancement. As shown in Fig. 5, the field dependence of the effective mass, detected by its Sommerfeld coefficient or by the resistivity coefficient A in T^2 dependence, shows a maximum at 12 T in URhGe and 14 T in UCoGe for $H \parallel b$-axis. On the other hand, the effective mass for the $H \parallel c$-axis decreases monotonously.

Assuming that T_{sc} basically follows the simplified McMillan-like formula, namely $T_{sc} \sim \exp[-(\lambda+1)/\lambda]$, T_{sc} will increase when the effective mass is enhanced. Here λ is related to the effective mass m^* and the band mass m_b, namely $m^* =$

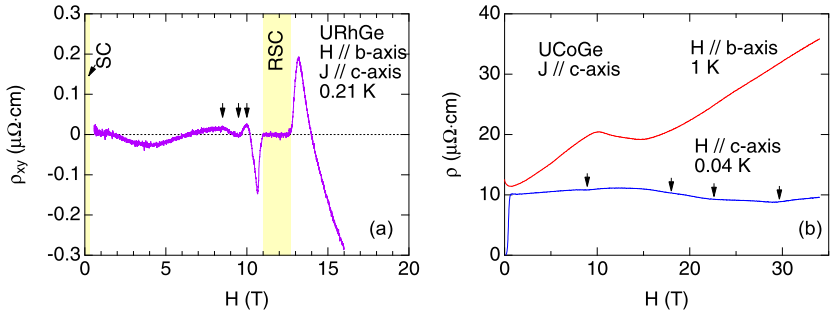

Fig. 6. (Color online.) (a) Field dependence of the Hall resistivity for the $H \parallel b$-axis in URhGe [23], and (b) magnetoresistance for the $H \parallel b$ and c-axis in UCoGe [28].

$m_b + m^{**} = (1+\lambda)m_b$. Since H_{c2} is governed only by the orbital limit in the spin-triplet state with equal spin pairing, one can describe H_{c2} as $H_{c2} \sim (m^* T_{sc})^2$. Therefore, if the effective mass is enhanced, T_{sc} will increase and, moreover, H_{c2} will increase. In this simple model, the field-reinforced (-reentrant) SC can be explained.

It should be noted that the decrease of effective mass for $H \parallel c$-axis in UCoGe is more drastic than that in URhGe. If we assume that the band mass is almost unchanged with increasing the field, the drop of effective mass is mainly due to the decrease of the correlation mass, namely m^{**}, which originates from the FM spin fluctuations. The correlation mass probably dominates the total effective mass in UCoGe, compared to the case in URhGe. This is also consistent with the fact that UCoGe is closer to the FM criticality.

5. Fermi surface instabilities

Up to now, we assumed that the Fermi surface is invariant under a magnetic field. In reality, the Fermi surface can be modified by the Zeeman spin splitting or the phase transition. In particular, UCoGe has a relatively low number of carriers and the Sommerfeld coefficient is moderately enhanced. Thus the magnetic field effect for the Fermi surface should be important. This can be easily understood considering the fact that the q factor ($\equiv S N_A e/(\gamma T)$), defined from the thermopower S and the specific heat γ-value, is relatively large, $q = 5$. The value is comparable to that in the low-carrier heavy fermion system URu_2Si_2, in which the Fermi surface is modified by the field, showing a Lifshitz transition [24–26].

The thermopower measurements for $H \parallel b$-axis in UCoGe show a maximum around 12 T at low temperatures, implying the reconstruction of the Fermi surfaces [27]. For the $H \parallel c$-axis, the magnetoresistance shows an anomaly at 9 T. Further increasing the field, successive anomalies at 18, 22 and 30 T are detected, as shown in Fig. 6b [28].

The low-field anomaly at 9T is also observed in the dHvA experiments. Figs. 7a–c show the dHvA oscillations and the corresponding FFT spectra. A clear anomaly is observed at $H^* = 9$ T in the dHvA oscillations for $H \parallel c$-axis. A single dHvA frequency is found in the FFT analysis with $F = 2.5 \times 10^6$ Oe at $H < H^*$, while the dHvA frequency splits into two above H^* probably due to the Zeeman spin-splitting, corresponding to the non-linear field response. The dHvA frequency F is proportional to the cross-sectional area of the Fermi surface S_F, namely $F = \hbar c/(2\pi e) S_F$. Assuming a spherical Fermi surface, the detected Fermi surface occupies only 0.2% of the Brillouin zone. The small splitting of the dHvA frequency indicates that the Fermi surface is most likely unchanged through H^*. The cyclotron effective mass below H^* is $11 m_0$, indicating a moderate enhancement in spite of the small frequency.

Although the dHvA effect and resistivity display the anomaly at H^*, the magnetization measurements at 1.5 K show no anomaly, indicating that the anomaly is very small; thus the usual magnetization measurements cannot detect it.

When the field direction is tilted from the c-axis, H^* increases rapidly, as shown in Fig. 7d. The dHvA frequency remains around 3×10^6 Oe for both $H < H^*$ and $H > H^*$, as shown in Fig. 7e–f, although it increases slightly with the field angle, indicating a nearly spherical Fermi surface.

A new frequency is observed at high field above 20 T in the Shubnikov–de Haas (SdH) experiments. Fig. 7g shows the angular dependence of SdH frequency. The frequency at high field is also almost constant, indicating a spherical Fermi surface. The frequency is around 1×10^7 Oe, which is larger than the dHvA frequency detected at low field. It occupies around 2% of the Brillouin zone. The corresponding γ-value obtained from this Fermi surface is 7 $mJ K^{-2} mol^{-1}$, which is more than 10% of the total γ-value at zero field. These results demonstrate the low carrier density with heavy electronic state in UCoGe.

At 1.5 GPa in the PM state, a similar dHvA frequency is observed. The SdH oscillations and its FFT are shown in Fig. 8. The detected frequency is 3×10^6 Oe, which is almost the same as the frequency detected at ambient pressure. The cyclotron mass for this frequency is $6.5 m_0$, which is smaller than that detected at ambient pressure. From these experiments, the Fermi surface seems unchanged, even in the PM state.

In the temperature–pressure phase diagram, T_{sc} smoothly changes as a function of pressure, with a broad maximum at P_c. When the Fermi surface is drastically reconstructed, T_{sc} also changes drastically, as observed in UGe_2 between FM1 and FM2 phases. The unchanged Fermi surface is consistent with the smooth change of T_{sc} around P_c. On the other hand,

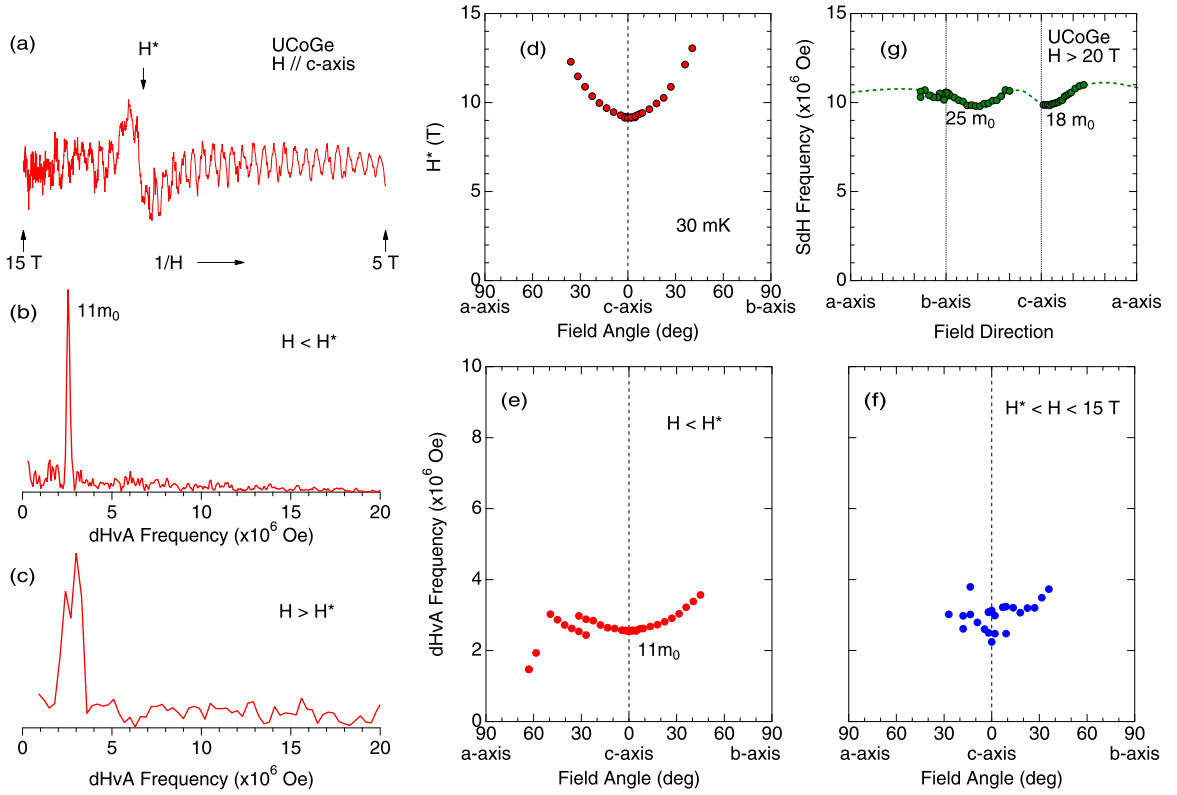

Fig. 7. (Color online.) (a) Typical dHvA oscillation and the corresponding FFT for (b) $H < H^*$ and (c) $H > H^*$ for the field along the c-axis at ambient pressure in UCoGe. (d) Angular dependence of H^* at low temperature. Angular dependence of dHvA frequency (e) below H^* and (f) above H^*. (g) Angular dependence of SdH frequency at very high field above 20 T. The cyclotron effective masses are determined as $11\,m_0$ for the $H \parallel c$-axis below H^*, and $25\,m_0$, $18\,m_0$ for the $H \parallel b$ and c-axis, respectively, above 20 T.

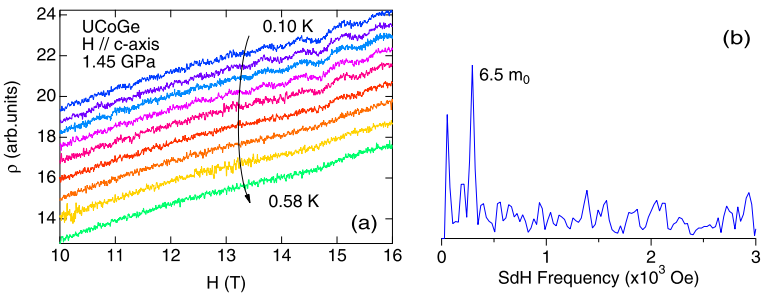

Fig. 8. (Color online.) Field dependence of magnetoresistance at different temperatures and the corresponding FFT at the lowest temperature at 1.45 GPa in the PM state in UCoGe. The cyclotron effective mass was determined to be $6.5\,m_0$.

T_{Curie} is the first order transition already at ambient pressure, according to the NQR experiments. The large difference of Fermi surfaces between PM and FM states is also predicted by the band calculations based on the 5f-itinerant model. The first-order nature of T_{Curie} should be continued for $T_{\mathrm{Curie}} \to 0$ K at P_c. Thus the drastic change of the Fermi surface is naturally expected. This is in contradiction with the present dHvA/SdH experimental results. Of course, not all the Fermi surface is detected here. Further experiments using higher-quality samples are required.

In URhGe, the results of SdH experiments are reported for the field direction slightly tilted from the b to the c-axis. [29] The detected SdH frequency is 5.5×10^6 Oe and the cyclotron effective mass is about $\sim 20\,m_0$ at 10 T at the field angle $\theta = 10$ deg. The γ-value, which is calculated from the detected SdH frequency, is 2.3 $\mathrm{mJ\,K^{-2}\,mol^{-1}}$, indicating a small contribution to the total γ-value, 160 $\mathrm{mJ\,K^{-2}\,mol^{-1}}$. The observed SdH frequency increases rapidly with the field, indicating a non-linear response of Zeeman splitting on the Fermi surface. The authors claim that the pocket Fermi surface vanishes near the reentrant-SC region, revealing a collapse of the Fermi velocity. In this case, the orbital limit increases strongly and the reentrant-SC can be explained. However, the detected Fermi surface is only a small pocket Fermi surface with a very small contribution (about 1.5%) to the total γ-value. In order to conclude on the relation between Fermi surface instability and reentrant-SC, the full determination of the Fermi surface is required using a higher-quality sample.

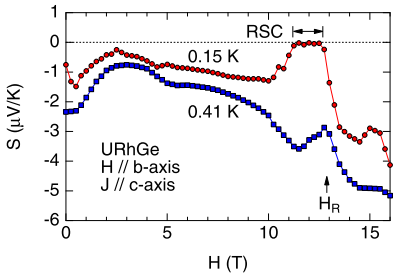

Fig. 9. (Color online.) Field dependence of thermoelectric power at 0.15 K and 0.41 K for $H \parallel b$-axis and the heat current direction $J \parallel c$-axis in URhGe.

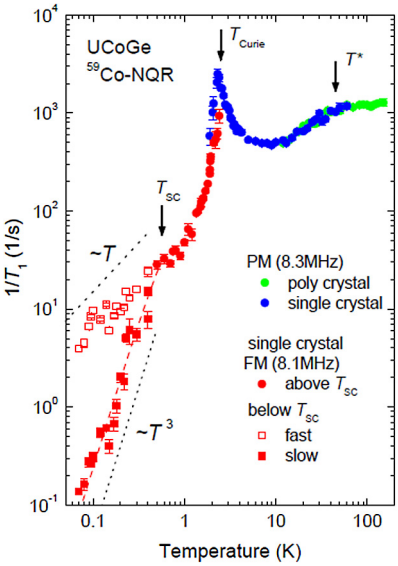

Fig. 10. (Color online.) Temperature dependence of $1/T_1$ in UCoGe [33].

Apart from the quantum oscillations, the Fermi surface instabilities are also suggested by Hall effect measurements. Fig. 6a shows the field dependence of the Hall resistivity. The slope of the Hall resistivity is quite different between low-field ($H < H_R$) and high-field ($H > H_R$) regions, implying that a drastic change in the Fermi surface. Moreover, small anomalies are detected at 10, 9.5 and 8.5 T, as denoted by arrows. These anomalies disappear at higher temperatures, above 0.4 K. The successive anomalies only at low temperatures in the transport measurements remind us the Lifshitz-type transitions observed in many heavy-fermion materials, such as URu_2Si_2 [26], $CeRu_2Si_2$ [30], $YbRh_2Si_2$ [31], where many anomalies are detected in the thermopower measurements near the (pseudo-) metamagnetic transition.

Our very recent results on thermopower measurements in URhGe are reminiscent of those in heavy fermion systems mentioned above. Fig. 9 shows the field dependence of thermopower at low temperatures for the $H \parallel b$-axis in URhGe. H_R and RSC correspond to the spin-reorientation field and the reentrant superconductivity, respectively. Other anomalies at least around 5 and 14 T are detected, although field definition for anomalies is not easy. Since the thermopower reflects the energy derivative of the density of state, it is a sensitive probe for Fermi surface modification. The results of thermopower measurements also imply the Fermi surface instabilities near H_R.

At zero field, recent ARPES studies on URhGe indicate the change of electronic structure below T_{Curie}, although it is not clear near the Fermi level due to the heavy flat band [32]. Hall effect measurements also show a change in the Hall coefficient in the FM state, indicating a change in the number of carriers. These results suggest that the Fermi surface is reconstructed in the FM state at zero field.

6. Dynamical studies: the case of UCoGe

New insights into the spin dynamics in UCoGe were obtained, as ^{59}Co is an excellent NMR probe. An evidence of the coexistence of SC and FM is well established by NQR [33]; it was also obvious in μSR experiments [34]. From the coexistence of PM and FM phases in a large T window below T_{Curie}, the FM transition must be a first-order one. However, in agreement with the tiny ordered FM moment ($m_0 \sim 0.05\,\mu_B$), the spin dynamics is dominated by slow energy spin fluctuations of the Ising type. At least just above T_{sc}, two relaxation components are detected, as shown in Fig. 10. The faster one displays a typical variation of a normal Fermi liquid phase with $1/T_1 \sim T$, the slower one displays a T^3 decrease on cooling, which

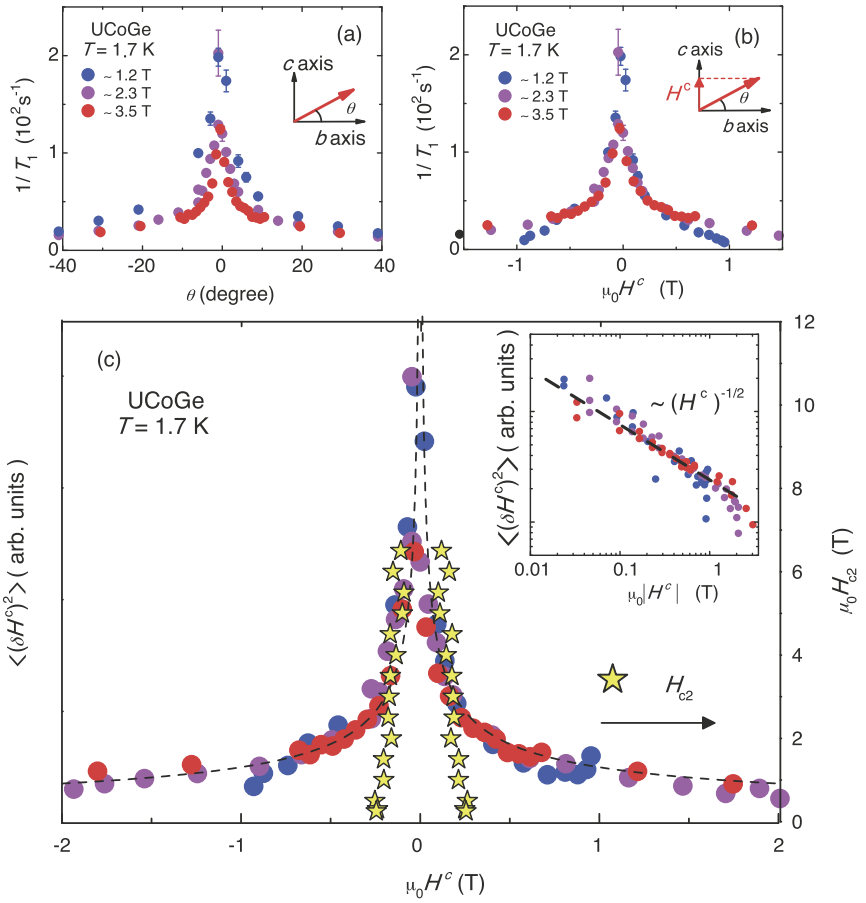

Fig. 11. (Color online.) (a) Angular dependence of $1/T_1$ and (b) H^c dependence of $1/T_1$. (c) FM fluctuations as a function of H^c [45].

is typical for unconventional SC with a line node. The surprising feature is that these two components have a comparable weight. The idea of self-induced vortex state by the internal field produced by FM has been invoked, but for such weak field the number of created vortices in volume must be small. Let us notice that the residual γ-term of specific heat of electronic origin appears weak for high-quality crystals [19]. Yet there is no understanding of SC inhomogeneity detected in NQR experiments.

As discussed previously, the key role of FM fluctuations appear in the strong anisotropy of the upper critical field $H_{c2}(0)$ observed in macroscopic experiments. From the specific heat measurements, the particular feature of UCoGe is that the Sommerfeld coefficient decreases drastically when the magnetic field is applied along the c-axis (easy axis), while its initial H dependence is weak for $H \parallel a$ and b-axes (hard axis), as shown in Fig. 5. These phenomena are beautifully observed in NMR experiments, as shown in Fig. 11. The maxima of $1/T_1$ occur for $H \parallel b$, i.e. for the angle θ of H versus the b-axis equal to 0. The key variable is the component for H along the c-axis; whatever the magnetic field H, $1/T_1$ depends only on the magnitude of its component along the c-axis (Fig. 11). As shown in Fig. 11c, the magnetic fluctuations $\langle(\delta H^c)^2\rangle$ have a singularity in $1/\sqrt{H^c}$ and a strong enhancement of $H_{c2}(0)$ is observed close to $H^c = 0$, i.e. for $H \parallel a$ and b (hard axes). Using the H dependence of the FM longitudinal fluctuations, excellent modeling of the H_{c2} anisotropy has been reproduced, assuming that the SC order parameter is the A state with point nodes with a d-vector near the Γ point. The strong H dependence of the fluctuations on H^c may be connected to the peculiar singularity of the Fermi surface.

In the case of URhGe, the new feature is that the initial decrease on H^c of the Sommerfeld coefficient is rather moderate. The major phenomenon when the field is applied along the b-axis is that this direction becomes the easy one at a critical field $H_R \sim 12$ T. There is evidence of H enhancement of the Sommerfeld coefficient. Basically the driving mechanism is that when the transverse field induces a magnetization comparable to the initial ordered moment ($0.7\,\mu_B$), its critical temperature drops and pushes the material close to FM instabilities. A crude model of superconductivity via effective mass enhancement at H_R gives an excellent fitting of the field reentrant superconductivity at zero pressure, and even regarding its evolution under pressure. Recently K. Hattori and H. Tsunetsugu have investigated theoretically reentrant superconductivity in the Ising superconductor URhGe under a transverse magnetic field [35]. In this model, soft magnons generate strong attractive interactions close to H_R when the FM component along c and the magnetic-field-induced magnetic component along b become comparable. A recent theoretical description of unconventional SC in uranium compounds can be found in Ref. [36].

The open question is the possible key role of the change of the Fermi surface topology at the FM–PM transition at zero field and also under a magnetic field, either in longitudinal or transverse configurations.

UGe_2 due to the high-quality single crystals is the only case where many Fermi surface orbits have been detected for the three different phases FM2, FM1, and PM [37,38]. Clear and large changes in the Fermi surfaces occur at P_x, P_c but also at H_x, H_m. For URhGe, only one small orbit has been detected; its disappearance just below H_R has been put forward to claim that it is the collapse of the Fermi surface that may explain the enhancement of H_{c2}. Recently, the indirect macroscopic evidence of Fermi surface reconstruction at H_R appears clear in Hall effect measurements as well as in thermopower measurements.

In UCoGe, only one orbit has been detected for $H \parallel c$. At least for the both URhGe and UCoGe, an H anomaly of the thermoelectric power has been detected when a singularity of H_{c2} is detected. Thus the underlining idea is that there are concomitant SC singularity and Fermi surface, such as a Lifshitz-like transition.

Maybe in these heavy-fermion compounds, where the local fluctuations play a leading role, SC is mainly given by short interactions and the role of the Fermi surface change can be interpreted as the consequence of the H variation of the Sommerfeld coefficient to describe the feedback on the SC pairing.

The key role of local fluctuation appears in neutron scattering experiments. Measurements on UGe_2 [39] and on UCoGe [40] point out that, opposite to the case of 3d itinerant systems, the damping rate is finite at the wave vector $q \to 0$. It has been emphasized that such a behavior is impossible in one type of carrier, because it would violate the spin conservation rule [41,42]. A new constant Γ_q as $q \to 0$ observed in UGe_2 and UCoGe is the signature of the interplay between localized and itinerant electrons in the phenomenological description as well as in the microscopic analysis. Other experimental evidences of two type of carrier were already given in μSR experiments for UGe_2 [43]. The electronic subset of itinerant states corresponds to a quite small moment with very slow spin dynamics. The μSR experiments under pressure has shown that this small moment contribution persists under pressure close to P_x [44]. Qualitative explanations on the experimental data are often made, assuming one carrier band. There is up to now no attempt to rebate the complexity of the Fermi surface and multiband character with the dual character observed on the spin dynamics.

Acknowledgements

This work was supported by ERC starting grant (NewHeavyFermion), French ANR project (CORMAT, SINUS, DELICE), KAKENHI, REIMEI and ICC-IMR.

References

[1] D. Aoki, J. Flouquet, J. Phys. Soc. Jpn. 81 (2012) 011003.
[2] Ø. Fischer, Magnetic Superconductors in Ferromagnetic Materials, Science Publishers BV, Amsterdam, 1990.
[3] S.S. Saxena, P. Agarwal, K. Ahilan, F.M. Grosche, R.K.W. Haselwimmer, M.J. Steiner, E. Pugh, I.R. Walker, S.R. Julian, P. Monthoux, G.G. Lonzarich, A. Huxley, I. Sheikin, D. Braithwaite, J. Flouquet, Nature 406 (2000) 587.
[4] D. Aoki, A. Huxley, E. Ressouche, D. Braithwaite, J. Flouquet, J.-P. Brison, E. Lhotel, C. Paulsen, Nature 413 (2001) 613.
[5] N.T. Huy, A. Gasparini, D.E. de Nijs, Y. Huang, J.C.P. Klaasse, T. Gortenmulder, A. de Visser, A. Hamann, T. Görlach, H.v. Löhneysen, Phys. Rev. Lett. 99 (2007) 067006.
[6] V. Taufour, D. Aoki, G. Knebel, J. Flouquet, Phys. Rev. Lett. 105 (21) (2010) 217201.
[7] H. Kotegawa, V. Taufour, D. Aoki, G. Knebel, J. Flouquet, J. Phys. Soc. Jpn. 80 (2011) 083703.
[8] F. Hardy, A. Huxley, J. Flouquet, B. Salce, G. Knebel, D. Braithwaite, D. Aoki, M. Uhlarz, C. Pfleiderer, Physica B 359 (2005) 1111.
[9] E. Hassinger, D. Aoki, G. Knebel, J. Flouquet, J. Phys. Soc. Jpn. 77 (7) (2008) 073703.
[10] E. Slooten, T. Naka, A. Gasparini, Y.K. Huang, A. de Visser, Phys. Rev. Lett. 103 (9) (2009) 097003.
[11] V.P. Mineev, C. R. Phys. 7 (2006) 35.
[12] D. Aoki, A. Huxley, F. Hardy, D. Braithwaite, E. Ressouche, J. Flouquet, J.P. Brison, C. Paulsen, Acta Phys. Pol. B 34 (2003) 503.
[13] A.P. Mackenzie, R.K.W. Haselwimmer, A.W. Tyler, G.G. Lonzarich, Y. Mori, S. Nishizaki, Y. Maeno, Phys. Rev. Lett. 80 (1998) 161.
[14] T. Ohta, Y. Nakai, Y. Ihara, K. Ishida, K. Deguchi, N.K. Sato, I. Satoh, J. Phys. Soc. Jpn. 77 (2008) 023707.
[15] D.E. de Nijs, N.T. Huy, A. de Visser, Phys. Rev. B 77 (2008) 140506.
[16] I. Sheikin, A. Huxley, D. Braithwaite, J.P. Brison, S. Watanabe, K. Miyake, J. Flouquet, Phys. Rev. B 64 (2001) 220503.
[17] F. Lévy, I. Sheikin, B. Grenier, A.D. Huxley, Science 309 (2005) 1343.
[18] D. Aoki, T.D. Matsuda, V. Taufour, E. Hassinger, G. Knebel, J. Flouquet, J. Phys. Soc. Jpn. 78 (2009) 113709.
[19] D. Aoki, J. Flouquet, J. Phys. Soc. Jpn. 83 (2014) 061011.
[20] V.P. Mineev, Phys. Rev. B 83 (6) (2011) 064515.
[21] F. Hardy, D. Aoki, C. Meingast, P. Schweiss, P. Burger, H.v. Loehneysen, J. Flouquet, Phys. Rev. B 83 (2011) 195107.
[22] W. Knafo, T.D. Matsuda, D. Aoki, F. Hardy, G.W. Scheerer, G. Ballon, M. Nardone, A. Zitouni, C. Meingast, J. Flouquet, Phys. Rev. B 86 (2012) 184416.
[23] D. Aoki, G. Knebel, J. Floquet, arXiv:1407.5799.
[24] H. Shishido, K. Hashimoto, T. Shibauchi, T. Sasaki, H. Oizumi, N. Kobayashi, T. Takamasu, K. Takehana, Y. Imanaka, T.D. Matsuda, Y. Haga, Y. Onuki, Y. Matsuda, Phys. Rev. Lett. 102 (15) (2009) 156403.
[25] D. Aoki, G. Knebel, I. Sheikin, E. Hassinger, L. Malone, T.D. Matsuda, J. Flouquet, J. Phys. Soc. Jpn. 81 (2012) 074715.
[26] A. Pourret, A. Palacio-Morales, S. Krämer, L. Malone, M. Nardone, D. Aoki, G. Knebel, J. Flouquet, J. Phys. Soc. Jpn. 82 (2013) 034706.
[27] L. Malone, L. Howald, A. Pourret, D. Aoki, V. Taufour, G. Knebel, J. Flouquet, Phys. Rev. B 85 (2012) 024526.
[28] D. Aoki, I. Sheikin, T.D. Matsuda, V. Taufour, G. Knebel, J. Flouquet, J. Phys. Soc. Jpn. 80 (2011) 013705.
[29] E.A. Yelland, J.M. Barraclough, W. Wang, K.V. Kamenev, A.D. Huxley, Nat. Phys. 7 (2011) 890.
[30] M. Boukahil, A. Pourret, G. Knebel, D. Aoki, Y. Ōnuki, J. Flouquet, Phys. Rev. B (2014), in press.
[31] A. Pourret, G. Knebel, T.D. Matsuda, G. Lapertot, J. Flouquet, J. Phys. Soc. Jpn. 82 (5) (2013) 053704.
[32] S.-i. Fujimori, I. Kawasaki, A. Yasui, Y. Takeda, T. Okane, Y. Saitoh, A. Fujimori, H. Yamagami, Y. Haga, E. Yamamoto, Y. Ōnuki, Phys. Rev. B 89 (2014) 104518.

[33] T. Ohta, T. Hattori, K. Ishida, Y. Nakai, E. Osaki, K. Deguchi, N.K. Sato, I. Satoh, J. Phys. Soc. Jpn. 79 (2) (2010) 023707.
[34] A. de Visser, N.T. Huy, A. Gasparini, D.E. de Nijs, D. Andreica, C. Baines, A. Amato, Phys. Rev. Lett. 102 (2009) 167003.
[35] K. Hattori, H. Tsunetsugu, Phys. Rev. B 87 (2013) 064501.
[36] V.P. Mineev, arXiv:1406.5030.
[37] T. Terashima, T. Matsumoto, C. Terakura, S. Uji, N. Kimura, M. Endo, T. Komatsubara, H. Aoki, Phys. Rev. Lett. 87 (16) (2001) 166401.
[38] R. Settai, M. Nakashima, S. Araki, Y. Haga, T.C. Kobayashi, N. Tateiwa, H. Yamagami, Y. Ōnuki, J. Phys. Condens. Matter 14 (2002) L29.
[39] A.D. Huxley, S. Raymond, E. Ressouche, Phys. Rev. Lett. 91 (2003) 207201.
[40] C. Stock, D.A. Sokolov, P. Bourges, P.H. Tobash, K. Gofryk, F. Ronning, E.D. Bauer, K.C. Rule, A.D. Huxley, Phys. Rev. Lett. 107 (2011) 187202.
[41] A.V. Chubukov, J.J. Betouras, D.V. Efremov, Phys. Rev. Lett. 112 (2014) 037202.
[42] V.P. Mineev, Phys. Rev. B 88 (2013) 224408.
[43] A. Yaouanc, P.D. de Réotier, P.C.M. Gubbens, C.T. Kaiser, A.A. Menovsky, M. Mihalik, S.P. Cottrell, Phys. Rev. Lett. 89 (2002) 147001.
[44] S. Sakarya, P.C.M. Gubbens, A. Yaouanc, P. Dalmas de Réotier, D. Andreica, A. Amato, U. Zimmermann, N.H. van Dijk, E. Brück, Y. Huang, T. Gortenmulder, Phys. Rev. B 81 (2010) 024429.
[45] T. Hattori, Y. Ihara, Y. Nakai, K. Ishida, Y. Tada, S. Fujimoto, N. Kawakami, E. Osaki, K. Deguchi, N.K. Sato, I. Satoh, Phys. Rev. Lett. 108 (2012) 066403.